JACS Au
AN OPEN ACCESS JOURNAL OF THE AMERICAN CHEMICAL SOCIETY

pubs.acs.org/jacsau
Article

Post-Transition-State Dynamic Effects in the Transmetalation of Pd(II)-F to Pd(II)-CF_3

Maoping Pu, Christian D.-T. Nielsen, Erdem Senol, Theresa Sperger, and Franziska Schoenebeck*

Cite This: *JACS Au* 2024, 4, 263−275
Read Online

ACCESS | Metrics & More | Article Recommendations | Supporting Information

ABSTRACT: The observation of post-transition-state dynamic effects in the context of metal-based transformation is rare. To date, there has been no reported case of a dynamic effect for the widely employed class of palladium-mediated coupling reactions. We performed an experimental and computational study of the trifluoromethylation of $Pd^{(II)}F$, which is a key step in the $Pd^{(0)}$/$Pd^{(II)}$-catalyzed trifluoromethylation of aryl halides or acid fluorides. Our experiments show that the *cis*/*trans* speciation of the formed $Pd^{(II)}CF_3$ is highly solvent- and transmetalation reagent-dependent. We employed GFN2-xTB- and B3LYP-D3-based molecular dynamics trajectory calculations (with and without explicit solvation) along with high-level QM calculations and found that depending on the medium, different transmetalation mechanisms appear to be operative. A statistically representative number of Born−Oppenheimer molecular dynamics (MD) simulations suggest that in benzene, a difluorocarbene is generated in the transmetalation with R_3SiCF_3, which subsequently recombines with the Pd via two distinct pathways, leading to either the *cis*- or *trans*-$Pd^{(II)}CF_3$. Conversely, GFN2-xTB simulations in MeCN suggest that in polar/coordinating solvents an ion-pair mechanism is dominant. A CF_3 anion is initially liberated and then rebinds with the $Pd^{(II)}$ cation to give a *cis*- or *trans*-$Pd^{(II)}$. In both scenarios, a single transmetalation transition state gives rise to both *cis*- and *trans*-species directly, owing to bifurcation after the transition state. The potential subsequent *cis*- to *trans* isomerization of the $Pd^{(II)}CF_3$ was also studied and found to be strongly inhibited by free phosphine, which in turn was experimentally identified to be liberated through displacement by a polar/coordinating solvent from the *cis*-$Pd^{(II)}CF_3$ complex. The simulations also revealed how the variation of the Pd-coordination sphere results in divergent product selectivities.

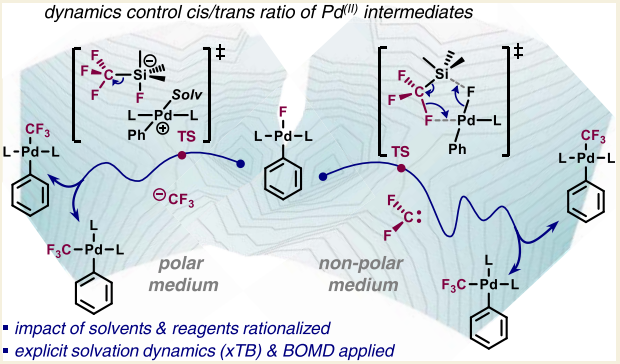

KEYWORDS: *transmetalation, computational, dynamic effect, palladium, trifluoromethyl*

1. INTRODUCTION

The advent and discovery of dynamic effects on reactivities have fundamentally changed conventional rationalizations and understanding,[1] as the region after the transition state dictates the product outcome in these cases, and as such, a single transition state may give rise to several products (i.e., in the so-called "bifurcation", see Figure 1A)[1bi] or multiple paths might be available from a transition-state region (in the so-called "roaming" phenomenon, see Figure 1B).[2] How the post-transition-state region affects the product outcome is currently still largely unknown and subject to intense research efforts.[1a3] Dynamic reactivity effects have been found to be crucial in numerous pericyclic reactions, especially cycloadditions and carbocation reactivities,[4] including examples that occur under enzyme catalysis.[5] The identification of such phenomena in the context of organometallic reactivities and catalysis is rare.[1d6]

To date, there is no reported dynamic reactivity effect in Pd-catalyzed cross-couplings. This reaction class belongs to the most impactful and most studied organometallic transformations,[7] and consists of various elemental steps, of which the transmetalation step is still the least well understood (Figure 1C).[8] This study focuses on the trifluoromethylation of $Pd^{(II)}$, which constitutes a key step in the $Pd^{(0)}$/$Pd^{(II)}$-catalyzed trifluoromethylation of aryl halides.[9] While this transformation is one of the most challenging transformations in the cross-coupling arena, with only three catalytic protocols of $Pd^{(0)}$/$Pd^{(II)}$-catalyzed trifluoromethylations existing to date,[9−11] it is also one of significant interest owing to the widespread industrial and academic interest in fluorinated molecules and fluorination methods.[12] The transmetalation step of $Pd^{(II)}$-X (where X is not F) is accompanied by the formation of reactive CF_3 anions, generated from the commonly used transmetalating agent R_3SiCF_3 in the presence of additives.[13,14] The CF_3 anions in turn

Received: November 17, 2023
Revised: December 11, 2023
Accepted: December 12, 2023
Published: December 29, 2023

https://doi.org/10.1021/jacsau.3c00724
JACS Au 2024, 4, 263−275

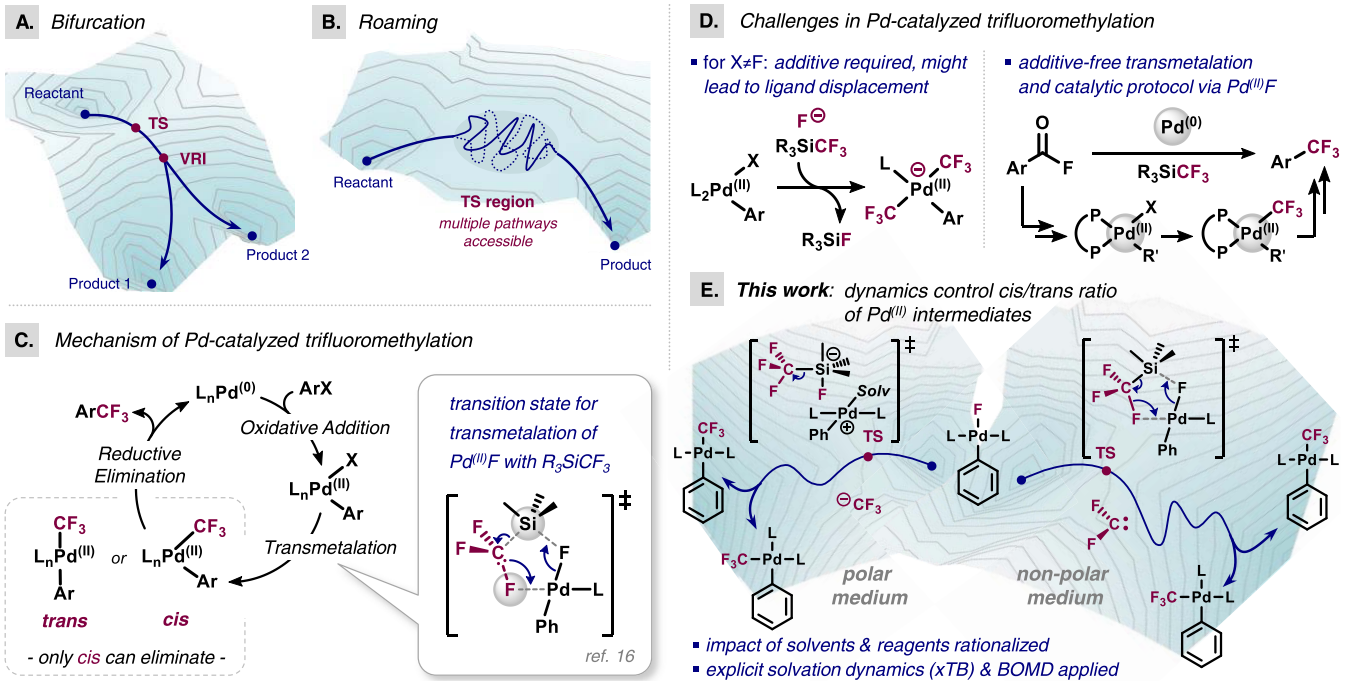

Figure 1. Dynamic effects: (A) bifurcation and (B) roaming. Pd-catalyzed trifluoromethylation: (C) catalytic cycle and previously identified transition state for transmetalation with Me_3SiCF_3; (D) importance of additive-free, direct transmetalation of $Pd^{(II)}$-F; and (E) this work.

can cause more weakly bound ligands to be displaced from $Pd^{(II)}$ and thus deactivate the catalyst.[13,15] If X = F on the other hand, transmetalation can take place directly without the need for exogenous additives,[15a] which avoids this detrimental side reaction and allows more weakly binding ligands for the similarly challenging reductive elimination[16] to be used. This concept was recently successfully leveraged in a catalytic protocol based on aromatic acid fluorides which yielded $ArCF_3$ upon additive-free decarbonylative trifluoromethylation[11] (via the key $Pd^{(II)}$-F intermediate) and related transformations,[17,18] see Figure 1D. As such, a precise understanding of the mechanism of the direct and additive-free transmetalation of $Pd^{(II)}F$ is critical to advance the further development of such catalytic protocols.

In this context, we recently communicated that the direct transmetalation of a $Pd^{(II)}F$ complex with trialkyl (trifluoromethyl) silane (R_3SiCF_3)[19] proceeds via an unusual transition state. In contrast to other transmetalations of $Pd^{(II)}$,[8,20] the reaction with $[L_1Pd^{(II)}(F)(Ar)]$ does not occur via a cyclic 4-membered transition state, but instead the CF_3−Si group is cleaved as to transfer only a fluoride to the palladium under liberation of a difluorocarbene (see Figure 1C).[19]

The CF_2 carbene then reacts with $Pd^{(II)}F$ to give the $Pd^{(II)}CF_3$ complex. We supported these findings experimentally by demonstrating that a separately synthesized difluorocarbene is directly reactive with $Pd^{(II)}F$ to give $Pd^{(II)}CF_3$. The mechanism was found to be independent of the phosphine ligand (L).

This manuscript describes our more comprehensive studies on the transmetalation mechanism as a function of reaction medium and transmetalating agent with a focus also on the resulting *cis*/*trans* speciation of the formed $Pd^{(II)}CF_3$ complex, which in turn is key for subsequent catalytic steps to happen. We show that the *cis*/*trans* distribution correlates with dynamic reactivity effects and that a single transmetalation transition state can result in *cis*- and *trans*-intermediates directly due to post-transition-state bifurcation.

2. RESULTS AND DISCUSSION

2.1. Experimental Studies of *Cis*/*Trans* Ratio of $Pd^{(II)}CF_3$ as a Function of Solvent and Reaction Partner

We set out to experimentally study the transmetalation of *trans*-$[(PPh_3)_2Pd^{(II)}(F)(Ph)]$ complex **1** with R_3SiCF_3 exclusively as well as a separately generated difluorocarbene as a function of solvent (Figure 2). We observed that difluorocarbene reacts with *trans*-$Pd^{(II)}F$ **1** to form the *trans*-$[(PPh_3)_2Pd^{(II)}(CF_3)(Ph)]$ (*trans*-**2**) complex exclusively, regardless of the solvent that was employed (i.e., benzene, DCM, and DMF gave analogous results, see Figure 2, top).

By contrast, our systematic investigation of *cis*/*trans* ratio for the transmetalation of *trans*-$[(PPh_3)_2Pd^{(II)}(F)(Ph)]$[21] **1** with Et_3SiCF_3 instead of the free difluorocarbene predominantly led to the *cis*-isomer (*cis*-**2**) in PhCN, DMF, and DMSO, whereas the *trans*-isomer (*trans*-**2**) was predominant in benzene (see Figure 2, bottom).

Interestingly, Grushin and co-workers previously also reported a solvent dependence on the *cis*/*trans* ratio in transmetalation with R_3SiCF_3 despite starting from the *trans*-precursor exclusively.[15a]

The origin of this solvent effect and the formation of *cis*-isomer, despite the *trans*-configuration of the precursor, is unexplained to date. On the other hand, monophosphines $[L_1Pd^{(II)}(CF_3)(Ar)]$ have been characterized and observed only in *cis*-configuration (with L = P*t*Bu_3, BrettPhos).[9,16a,22]

Our systematic analysis of the transmetalation of **1** with Et_3SiCF_3 over time showed that in the polar solvents PhCN or DMF, the reaction was rapid (being complete in less than 10 min) and that the initially set *cis*/*trans* ratio remained configurationally stable over 24 h at room temperature. By contrast, the same process in benzene proceeded more slowly (evolving over 24 h) and the *cis*/*trans* ratio changed over time from an initial 1:3 ratio (after 10 min and 1 h) to nearly complete observation of the *trans*-$Pd^{(II)}CF_3$ after 24 h (Figure 2). While

https://doi.org/10.1021/jacsau.3c00724
JACS Au 2024, 4, 263−275

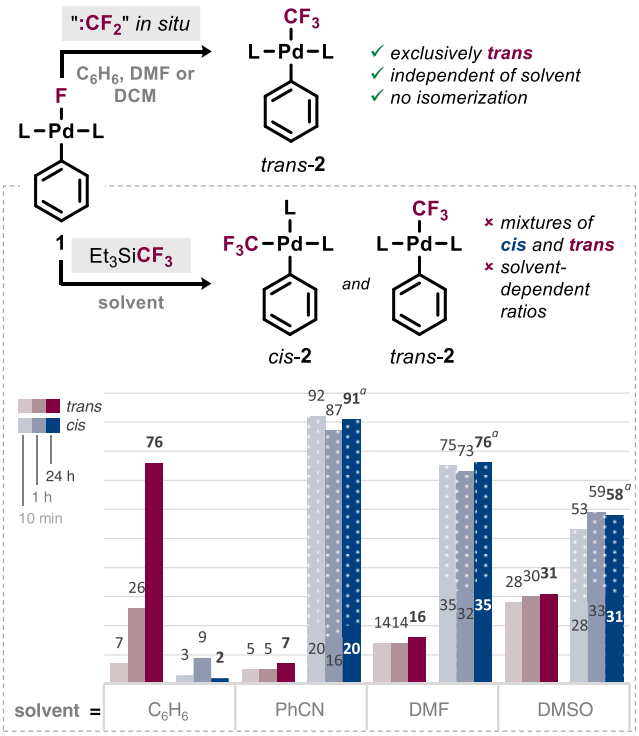

Figure 2. Transmetalation with CF_2 generated in situ (top) vs Et_3SiCF_3 (bottom) with **1** in different solvents after 10 min, 1 h, and 24 h. L = PPh_3 [a] including exchange of one L by solvent (vide infra).

the observations in the nonpolar solvents suggest that *cis*-to-*trans* isomerization can occur as a competitive process to the transmetalation, the different reaction outcomes observed in the polar media for the different transmetalating agents, i.e., Et_3SiCF_3 (giving predominantly *cis*) vs CF_2 carbene (giving exclusively *trans*), are particularly striking and imply that the *cis*/*trans* ratios at room temperature under these conditions do not arise from isomerization or thermodynamic equilibration of the product $Pd^{(II)}CF_3$ complexes.

2.2. Experimental Investigation of the Isomerization of the $L_nPd^{(II)}(CF_3)(Ph)$ Complex

We set out to separately synthesize the *cis*-$[(PPh_3)_2Pd^{(II)}(CF_3)(Ph)]$ complex to gain greater insight of its potential to isomerize to the corresponding *trans*-complex. To date, only the corresponding *trans*-complex had been made and/or characterized. To access the *cis*-complex, we first prepared the literature known tmeda-coordinated precursor (tmeda = tetramethylethylenediamine), i.e., *cis*-$[(tmeda)Pd^{(II)}(CF_3)(Ph)]$[23] and subsequently displaced tmeda with two equivalents of PPh_3. To our delight, the displacement was stereospecific, resulting in the first synthesis (and characterization) of the *cis*-$[(PPh_3)_2Pd^{(II)}(CF_3)(Ph)]$ complex (*cis*-**2**). See Figure 3 for the synthesis and X-ray crystallographic support.[24]

With the *cis*-**2** complex in hand, we studied its isomerization to the *trans*-complex as a function of solvent. Interestingly, while we observed a relatively short half-life ($t_{1/2}$ = 19 min) and low isomerization barrier in benzene (experimentally determined as $\Delta G^{\ddagger}$ = 23.7 kcal/mol), we observed a much slower isomerization in acetonitrile and DMF, with only 6% *trans*-$Pd^{(II)}CF_3$ being formed within 36 h at room temperature in DMF. These results are consistent with the above observations that the established *cis*/*trans* ratio remained configurationally stable for 24 h at room temperature for DMF and PhCN, but

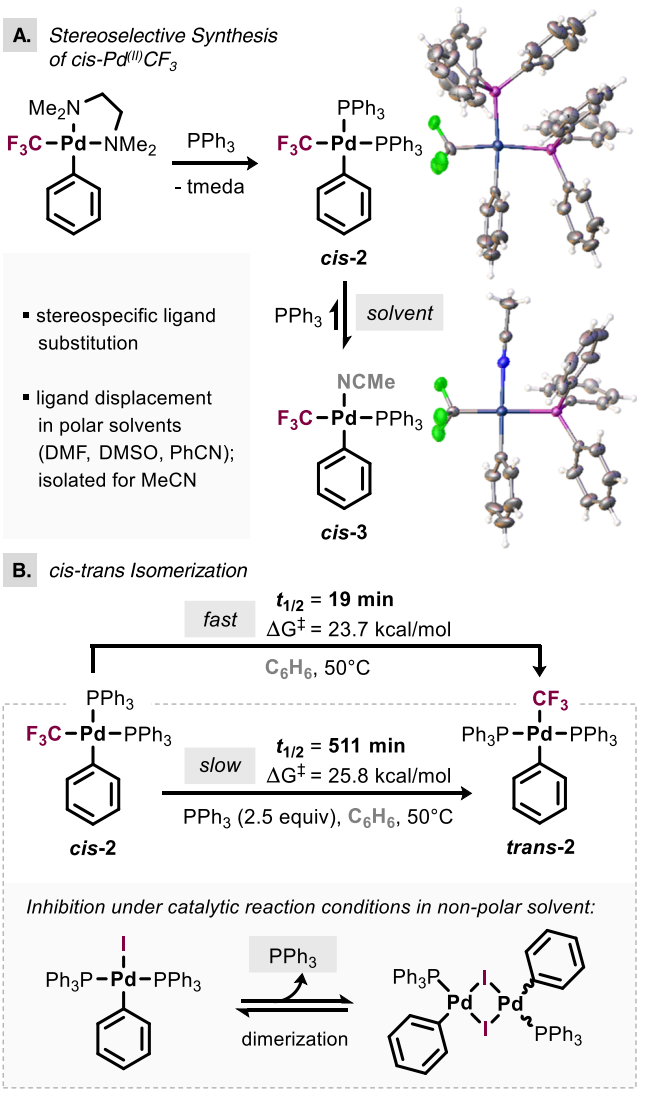

Figure 3. Independent synthesis of *cis*-**2** by ligand substitution and subsequent reactivity with solvent as well as X-ray structures of *cis*-**2** and *cis*-**3**.[24]

isomerization occurred in benzene as the transmetalation proceeded.

Interestingly, we also observed that the *cis*-$Pd^{(II)}CF_3$ complex partially exchanges a phosphine ligand for a solvent molecule in the polar solvents (57% observed in DMF, 68% observed in MeCN), see Figure 2. The *trans*-$Pd^{(II)}CF_3$ (as well as *trans*-$Pd^{(II)}F$ starting complex **1**), on the other hand, does not undergo a solvent/ligand exchange and remains unchanged in all solvents.

Since the isomerization requires an initial dissociation of a phosphine ligand, followed by isomerization from *cis*- to *trans*-$Pd^{(II)}CF_3$ from the tricoordinate, monophosphine complex, we speculated that the origin of slower isomerization in polar solvent might stem from the excess phosphine that is liberated upon formation of the solvent-coordinated *cis*-$Pd^{(II)}CF_3$ complex *cis*-**3**. Indeed, when we studied the *cis*–*trans* isomerization of *cis*-$Pd^{(II)}CF_3$ (*cis*-**2**) in the presence of 2.5 equiv of PPh_3 in benzene, we saw the isomerization being significantly slowed and we observed only 2% conversion to the *trans*-$Pd^{(II)}CF_3$ (*trans*-**2**) after 36 h at room temperature (50% conversion to *trans*-**2** after 9 h at 50 °C). We determined the

https://doi.org/10.1021/jacsau.3c00724
JACS Au 2024, 4, 263−275

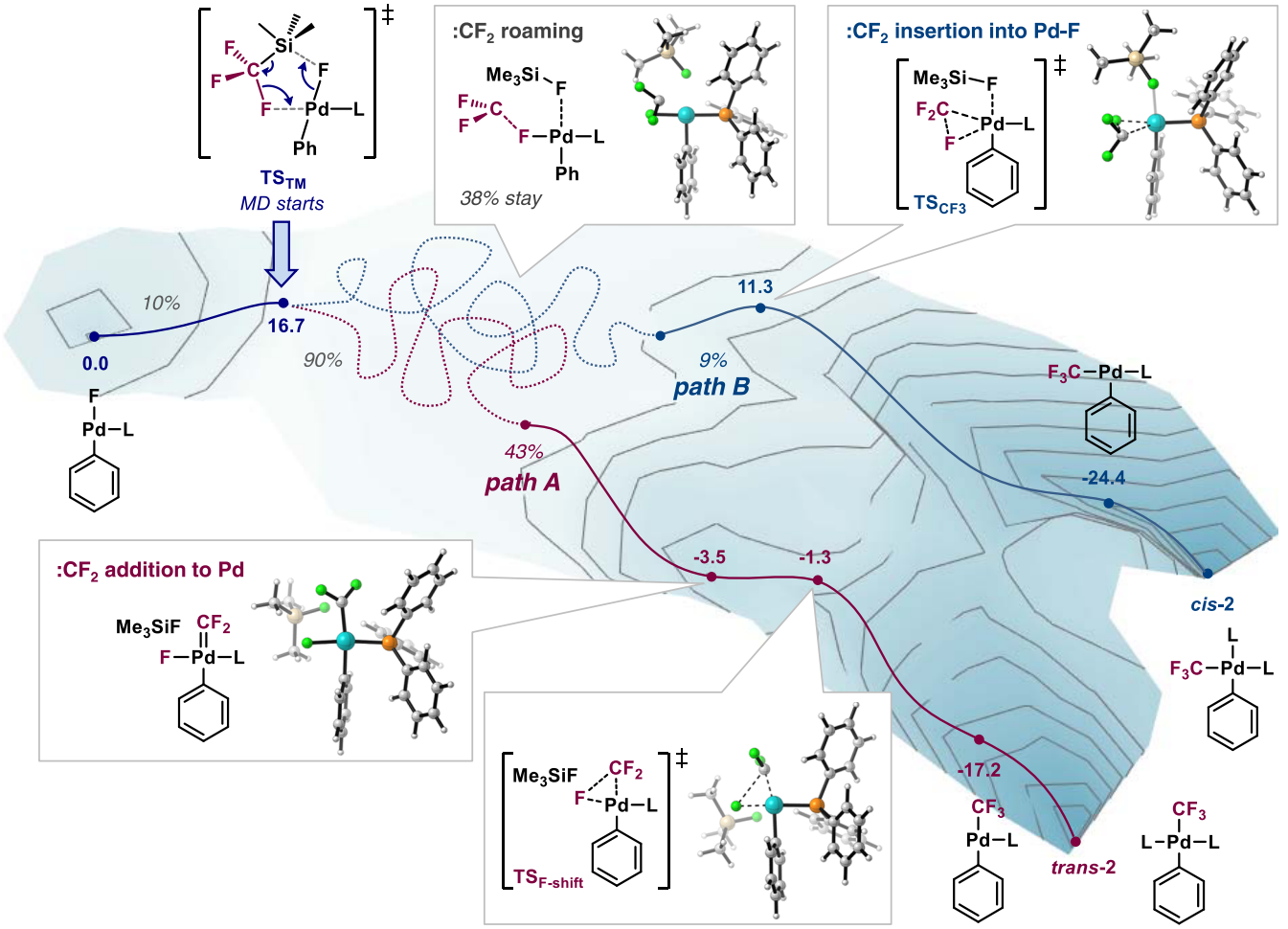

Figure 4. Outcome of 100 BOMD trajectory calculations after 5 ps starting from TS_{TM} in the transmetalation of *trans*-[$(PPh_3)Pd^{(II)}(F)(Ph)$] with Me_3SiCF_3. B3LYP-D3/6-31G(d) was used for BOMD. Energies (in kcal/mol) refer to Gibbs free energies obtained after optimization of key points (of the dynamics simulation) at the SMD (benzene) M06L/def2-TZVP//B3LYP-D3/6-31G(d,p), SDD(Pd) level of theory. L = PPh_3. [See also the Supporting Movies (S1 and S2) of these processes.] Reproduced with simulations in ORCA as an NVT ensemble at 300 K.[32]

experimental activation barrier of $\Delta G^{\ddagger}$ = 25.8 kcal/mol ($t_{1/2}$ = 511 min) for isomerization in the presence of excess PPh_3 in benzene.

Extrapolated to catalytic reaction conditions, where $Pd^{(II)}$ intermediates are only formed in small quantities and coexist with other species, excess ligand could well be encountered and post-transmetalation isomerization hence be of low(er) significance. In this context, our additional tests with added water or Et_3SiCF_3 showed no effect on the extent and speed of isomerization. In stark contrast, the presence of [$(PPh_3)_2Pd^{(II)}(I)(Ph)$] (which is the precursor to the "transmetalation-active" $Pd^{(II)}F$ complex, and would likely coexist in a catalytic context) was found to suppress the *cis*−*trans* isomerization of the $Pd^{(II)}CF_3$ complex when we studied the transmetalation. We speculate that this is due to its known dynamic equilibrium to form a $[(PPh_3)_1Pd^{(II)}(I)(Ph)]_2$ dimer,[25] which would liberate a ligand that in turn inhibits the isomerization. These observations imply that *cis*−*trans* isomerization under catalytic reaction conditions may be of lower significance in nonpolar solvents than encountered under stoichiometric conditions. On the other hand, the observation of the ability of polar/coordinating solvent to displace PPh_3 is of importance also for the effectiveness of a ligand to trigger the challenging subsequent reductive elimination.

Overall, these data confirm that the observed *cis*/*trans* speciation (especially at the early stages of conversions) cannot be rationalized through thermodynamic considerations and *cis*/*trans* isomerization of the $Pd^{(II)}CF_3$ complex. Instead, the *cis*/*trans* geometry appears to be set at the preceding transmetalation event. We therefore set out to gain more detailed information on the transmetalation under various mechanistic scenarios.

2.3. DFT-Based Born−Oppenheimer Molecular Dynamics (BOMD) Simulations of the "Difluorocarbene Pathway" (From R_3SiCF_3 or Free "CF_2") in the Gas Phase

As our prior studies had shown that the direct transmetalation of a monophosphine [$L_1Pd^{(II)}(F)(Ph)$] complex with Me_3SiCF_3 involves an unusual transmetalation TS in which difluorocarbene is released (see Figure 1C), which subsequently recombines with the Pd, we reasoned that an analysis of a representative number of reaction trajectories for this recombination would be useful to gain a comprehensive reactivity picture.

The monophosphine complex would be representative of P*t*Bu_3 and BrettPhos that react via monophosphine catalytic intermediates. Similarly, previous studies of the transmetalation of [$L_2Pd^{(II)}(X)(Ar)$] complexes concluded that a palladium bisphosphine complex initially undergoes dissociation of one

https://doi.org/10.1021/jacsau.3c00724
JACS Au 2024, 4, 263−275

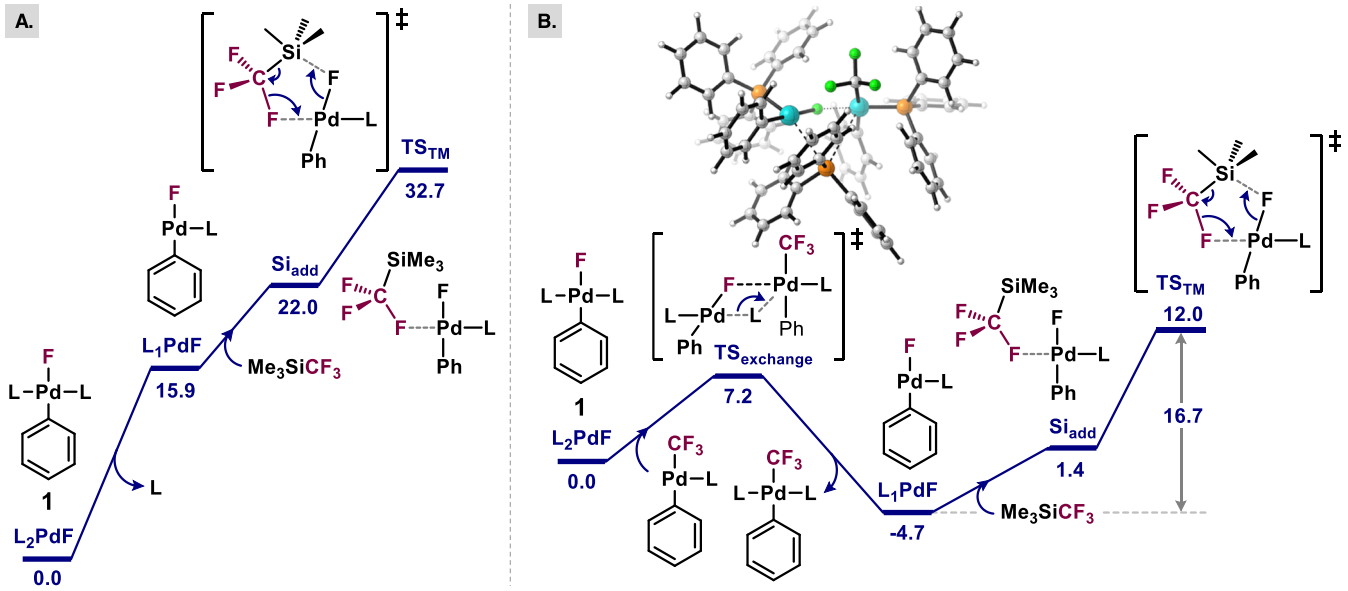

Figure 5. (A) Barrier to reach TS_{TM} under dissociation of ligand. (B) Alternative pathway to react via the same TS_{TM} by transferring ligand to another $Pd^{(II)}$. Energies (in kcal/mol) refer to Gibbs free energies at the SMD (benzene) M06L/def2-TZVP//B3LYP-D3/6-31G(d,p), SDD(Pd) level of theory (L = PPh_3).

ligand (L) upon interaction with the transmetalation agent to create an open coordination site.[26] Thus, detailed information on the monophosphine $[L_1Pd^{(II)}(F)(Ar)]$ complex would be valuable for further interpretation. Using Born−Oppenheimer molecular dynamics (BOMD),[27] we set out to run MD trajectories at room temperature from the initial transmetalation transition state (TS_{TM}), which releases the difluorocarbene. We initially ran 100 trajectories (in the gas phase), starting from the key transmetalation transition state TS_{TM} (see Figure 4) using B3LYP-D3/6-31G(d) level of theory (see the Supporting Information on the precise parameters of dynamics simulations).[28] We calculated the full complex; no simplifications were applied. At the B3LYP-D3/6-31G(d) level of theory, a single trajectory calculation of 5 ps took about 6 days of running time on one of our supercomputers (CPU: Intel Broadwell EP with 24 cores), showcasing that such demanding calculations are nowadays feasible.

Of the 100 calculated trajectories, 10% fell back to the reactant $Pd^{(II)}F$ complex **1**, the remaining 90% of trajectories led to a liberation of the difluorocarbene in the transition state TS_{TM} at about 200 fs (via $Me_3Si\cdots CF_2\cdots F$ cleavage, see Figure 4).[29]

The $:CF_2$ then weakly associates with the Pd complex but overall shows an extensive and random-like motion. In other words, the difluorocarbene "roams". Overall, 52 trajectories ultimately led to the product $Pd^{(II)}CF_3$ **2** within 2−5 ps simulation time, while the remaining 38 trajectories had retained "free difluorocarbene" at the time of termination of simulation (i.e., after 5 ps).

Interestingly, for the recombination of $:CF_2$ with $Pd^{(II)}F$, the dynamics revealed two different pathways that overall lead to the two different $Pd^{(II)}CF_3$ complex configurations, i.e., *cis* and *trans*. In one pathway (red in Figure 4), the difluorocarbene initially binds to the palladium center to produce the $[Pd^{(II)}] = CF_2$ complex, which is followed by a 1,2-fluoride shift to generate the *trans*-$[(PPh_3)Pd^{(II)}(CF_3)(Ph)]$ (*trans*-**2**).[30] In the other pathway (blue in Figure 4), the difluorocarbene directly attacks the fluoride on the Pd center, generating *cis*-$[(PPh_3)Pd^{(II)}(CF_3)(Ph)]$ (*cis*-**2**). The blue pathway underwent 17% of the productive trajectories and the red pathway in 83% of the product-forming trajectories. [Movies S1 and S2 of these pathways are provided as the Supporting Information for clarity and visualization].

These results were obtained through Gaussian's BOMD implementation as an NVE ensemble.[31] To more closely resemble experimental conditions, we also ran 100 trajectories using ORCA[32] under NVT conditions at room temperature (300 K), which resulted in the analogous 3:1 distribution of *trans*- and *cis*-**2** (see the SI for additional information).[33]

To gain quantitative information about the free energies of the simulated pathways, we also turned to high-level DFT calculations and explored the crucial stationary points observed during BOMD simulations (see Figure 4). At the SMD (benzene) M06L/def2-TZVP level of theory,[34] the critical transmetalation TS_{TM} is 16.7 kcal/mol in energy. We calculated transition states for the subsequent difluorocarbene attack directly at PdF relating to the blue path, which is at 11.3 kcal/mol (relative to the starting $[L_1Pd^{(II)}(F)(Ph)]$ and hence lies 5.4 kcal/mol below TS_{TM}). The red path via initial difluorocarbene attack at $Pd^{(II)}$, followed by a 1,2-F shift is calculated to have the highest energy point at −1.3 kcal/mol. The direct Pd−F insertion is thus $\Delta\Delta G^{\ddagger}$ = 12.6 kcal/mol higher in energy than the $TS_{F\text{-shift}}$ of the competing path. Clearly, any rationalization with a Curtin−Hammett analysis or transition-state theory would conclude that the blue path would not be undergone. However, since TS_{TM} is higher in energy than any subsequent TS, there is sufficient energy "in the system" to access the subsequent TSs; characteristic of reactivity scenarios that are dictated by nonstatistical dynamic effects.

The starting $[L_1Pd^{(II)}(F)(Ph)]$ can overall exist in two different T-shape configurations. Our calculations suggest that the energy difference between the two T-shaped configurations is small (1.1 kcal/mol); transmetalation via TS_{TM} is favored however (by $\Delta\Delta G^{\ddagger}$ = 0.8−2.1 kcal/mol, depending on method and solvent, see the SI for further details). We also launched BOMD trajectory runs for the higher-energy isomeric transition state (i.e., resulting from the alternative T-complex) and

https://doi.org/10.1021/jacsau.3c00724
JACS Au 2024, 4, 263−275

observed the analogous post-transition-state dynamic effect, resulting in *cis*- and *trans*-$Pd^{(II)}CF_3$ complexes also.

The overall selectivity will therefore be a Boltzmann-weighted average of the post-transition-state dynamic effects of all accessible transition-state isomers of TS_{TM} (which is predominantly dictated by the lowest-energy TS_{TM} here).

Although the trajectory calculations suggest that a distribution of *cis* and *trans* complexes of $[L_1Pd^{(II)}(CF_3)(Ar)]$ results after transmetalation with R_3SiCF_3, the known monophosphine $Pd^{(II)}CF_3$ complexes [such as (BrettPhos)$Pd^{(II)}(CF_3)(Ar)$] have been experimentally detected solely as *cis*.[9] In line with this, our calculations of the monophosphine $[(PPh_3)$-$Pd^{(II)}(CF_3)(Ph)]$ showed that there is a clear preference for the T-shaped complex that has CF_3 and phenyl *cis* to each other.[22] The preference for the *cis*-complex is very pronounced (>6 kcal/mol) and was found to be independent of solvent (see Figure 5A and Table S7 in the SI). Moreover, the activation free-energy barrier from *trans* to *cis* was also calculated to be relatively small, requiring only $\Delta G^{\ddagger}$ = 9.1 kcal/mol. These data suggest that although post-transition-state dynamic effects were observed, a monophosphine $[L_1Pd^{(II)}(CF_3)(Ar)]$ species will generate the *cis*-configuration, unless the isomerization process is outcompeted (see below).

Transmetalation of a bisphosphine $[L_2Pd^{(II)}(F)(Ar)]$ complex as experimentally studied.

Given the calculated facile isomerization of a monophosphine $Pd^{(II)}$ complex, the dynamically observed *cis*/*trans* distribution after TS_{TM} should only be of relevance if either no complete dissociation of one phosphine or very rapid "trapping" of the generated *cis*-monophosphine Pd species takes place. As we will discuss below, the "trapping" indeed appears to be feasible.

It is widely assumed that transmetalation of a bisphosphine complex would involve the initial formation of a monophosphine $[L_1Pd^{(II)}(F)(Ar)]$; in line with frequent assumptions that transmetalation at $Pd^{(II)}$ with typical transmetalating reagents would require an open coordination site.[8ad35] Our previous computational studies with complex **1** supported that ligand dissociation, followed by transmetalation with R_3SiCF_3 via TS_{TM} is favored over the corresponding alternatives, such as direct transmetalation without ligand dissociation.[19]

Consistent with this view, we saw inhibition of transmetalation of complex **1** with R_3SiCF_3 in benzene when excess PPh_3 (10 equiv) was added. The activation free-energy barrier for the transmetalation of $[L_1Pd^{(II)}(F)(Ph)]$ is calculated to be 16.7 kcal/mol (Figure 4), which is consistent with the observed transmetalation at room temperature. However, when the initially required ligand dissociation from $[L_2Pd^{(II)}(F)(Ar)]$ is included in the energetic consideration, the overall activation free-energy barrier rises to 32.7 kcal/mol in benzene (Figure 5A), which is high for the relatively facile reactivity seen in benzene. While the quantitative reproduction of ligand dissociation/association events with DFT has historically been challenging,[34] this high barrier could potentially originate from computational limits. Of our assessment of various computational methods, solvation models and basis sets gave free energies ranging from 15 to 26 kcal/mol for the dissociation of PPh_3 from $[L_2Pd^{(II)}(F)(Ph)]$ in benzene.[36] We include a more detailed discussion on this point in the Supporting Information (see page S28 f).

Alternatively, the transmetalation of $[L_2Pd^{(II)}(F)(Ph)]$ complex **1** might not proceed through dissociation of PPh_3 to form $[L_1Pd^{(II)}(F)(Ph)]$. If a small amount of $[L_1Pd^{(II)}(F)(Ph)]$ were to be formed, subsequently undergoing transmetalation, the formed $[L_1Pd^{(II)}(CF_3)(Ph)]$ is calculated to have a greater affinity for PPh_3 than $Pd^{(II)}F$. In other words, our calculations show that the abstraction of a ligand from $[L_2Pd^{(II)}(F)(Ph)]$ by $[L_1Pd^{(II)}(CF_3)(Ph)]$ should kinetically and thermodynamically readily occur, which would constitute an alternative generation of $[L_1Pd^{(II)}(F)(Ar)]$ that is energetically much more feasible (see Figure 5B).

Notably, the ligand abstraction with 7.2 kcal/mol is calculated to be more facile than the corresponding isomerization of a monophosphine $Pd^{(II)}$ complex (9.1 kcal/mol). As such, the observed *cis*/*trans* speciation through dynamic reactivity events could indeed be "trapped" through the ligand exchange.

Could a pathway that does not involve transmetalation also play a role?

The dynamics calculations showed that after 5 ps of simulation, some difluorocarbene was still "roaming". Although we did not observe it in the simulation, there is in principle the possibility that it eventually might also escape from the Pd sphere and recombine with another complex of **1**. However, since the experiments of **1** with separately generated difluorocarbene exclusively led to the *trans*-$PdCF_3$ complex (regardless of the employed solvent), any "escaped" difluorocarbene should also give rise to *trans*-$PdCF_3$. Moreover, Me_3SiCF_3 can also be a source of difluorocarbene, although this has been observed primarily in the presence of additives,[14] while our study is additive-free. Again, the *trans*-complex would result and the formation of the *cis*-$PdCF_3$ complex would not be accounted for in such scenarios.

The direct transmetalation of L_1PdF, and post-transition-state speciation, followed by rapid trapping of the resulting species with phosphine is fully consistent with the observed early product distribution in nonpolar medium. Subsequently, as discussed above *cis*/*trans* isomerization can take place in nonpolar medium, unless excess ligand is present.

We next investigated the dynamic reactivity of "free difluorocarbene" reaction conditions, in which we had generated $:CF_2$ in situ from a suitable precursor reagent and subjected it to *trans*-$[(PPh_3)_2Pd^{(II)}(F)(Ph)]$ **1** (Figure 2). To this end, we started BOMD simulations from the reactant complex of **1** together with CF_2. Overall, we ran 20 simulations, of which 7 were productive (Figure 6). We observed that all productive trajectories exclusively proceeded via the direct Pd−F attack pathway and hence led to the *trans*-product, i.e., *trans*-$[(PPh_3)_2Pd^{(II)}(CF_3)(Ph)]$ **2**. These results are in full agreement with our experimental results that gave *trans*-**2** exclusively, regardless of the reaction medium. Since the bisphosphine complex, $[(PPh_3)_2Pd^{(II)}(F)(Ph)]$ **1**, remained intact during the

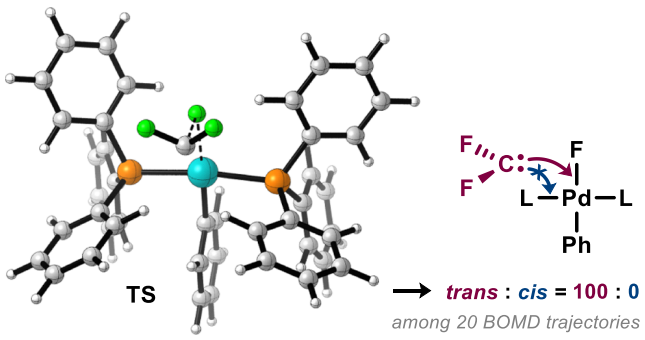

Figure 6. BOMD for blocked Pd-coordination sphere by a ligand with difluorocarbene $:CF_2$ leading to direct Pd−F insertion.

https://doi.org/10.1021/jacsau.3c00724
JACS Au 2024, 4, 263−275

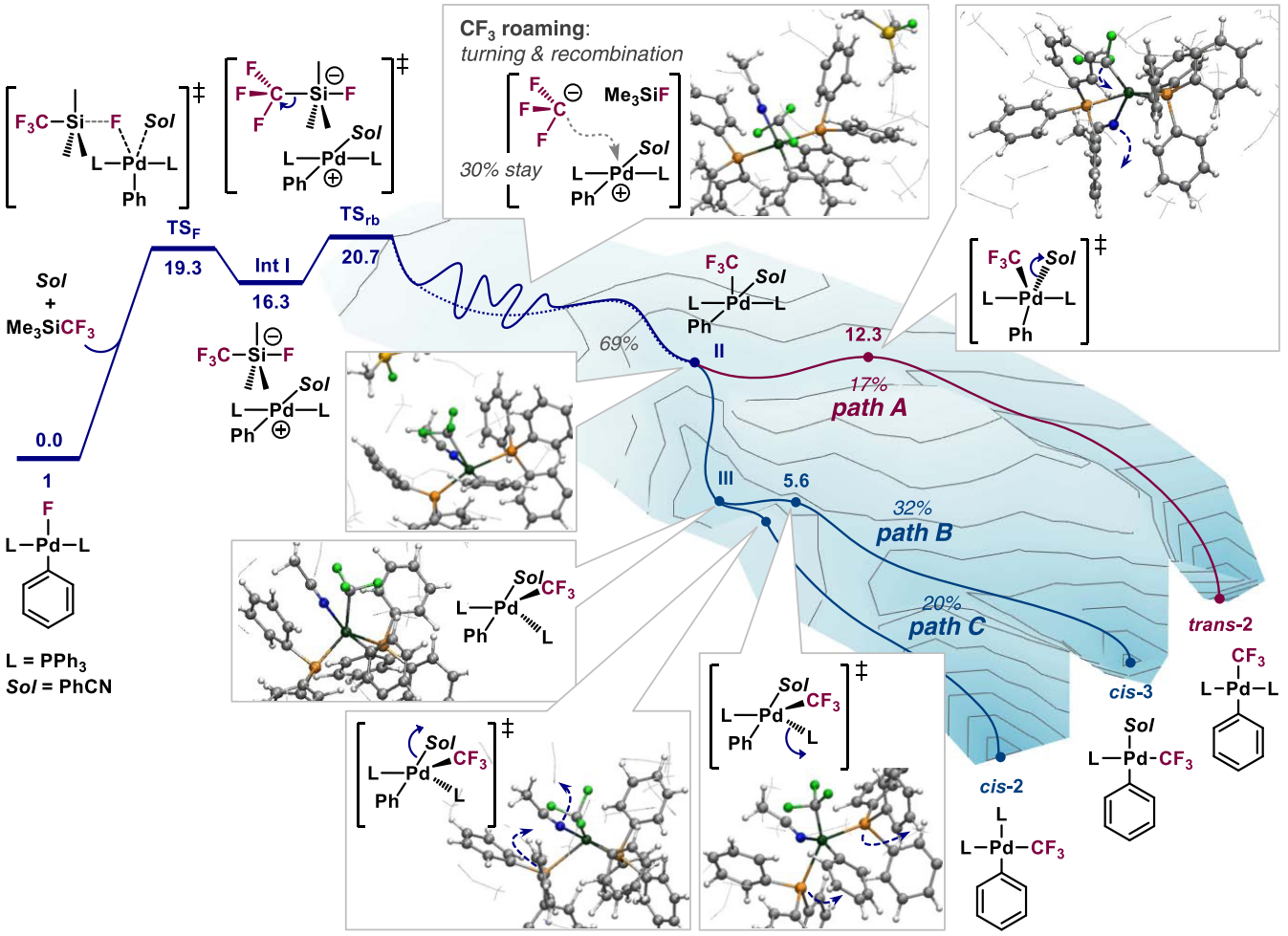

Figure 7. Transmetalation of Me_3SiCF_3 to $[(PPh_3)_2Pd^{(II)}(Ph)F]$ complex **1** in polar solvents (in benzonitrile): Results of xTB trajectory calculations and localization of stationary points at the SMD (PhCN) M06L/def2-TZVP//B3LYP-D3/6-31G(d,p),SDD(Pd) level of theory constructed based on the reactive events from molecular dynamics simulations. Representative snapshots from MD simulations (conducted with xTB; *Sol* = MeCN) in 50 MeCN molecules. [See also the Supporting Movies (S3−S6) of these processes]. Results were reproduced with DFT-based BOMD in ORCA (100 trajectories, NVT ensemble, 300 K, with only a single explicit solvent molecule; Sol = PhCN).

simulation, all coordination sites were blocked, and as such, the only available reaction channel for the difluorocarbene was that resulting from direct Pd−F bond insertion. This reactivity is independent of the reaction medium (solvent), corroborating the experimentally observed solvent indifference.

A key difference between transmetalation with R_3SiCF_3 and "free difluorocarbene" reactivity, therefore, appears to originate from the different coordination sphere and available reaction pathways.

2.4. Polar Solvent—Alternative Mechanism? GFN2-xTB Molecular Dynamics Simulations

While the above data and discussion indicate post-transition-state dynamic effects in the transmetalation of $Pd^{(II)}$-F with R_3SiCF_3, a key experimental observation is not yet fully accounted for. For the transmetalation of $[(PPh_3)_2Pd^{(II)}(Ph)(F)]$ **1** in Figure 2, we observed that while reactions with R_3SiCF_3 in benzene proceeded rather slowly over time, evolving over the course of 24 h at room temperature, the transmetalation in PhCN, DMF, and DMSO by contrast was very rapid and had already completed within 10 min (to give high *cis*-selectivity).

Our calculations of the transmetalation barrier for the various different media with implicit solvation suggest no pronounced effect on the initial transition state, TS_{TM}, with $\Delta\Delta G^{\ddagger}$ being only 0.5 kcal/mol for transmetalation in benzonitrile vs benzene.

The difference of reaction speed might therefore potentially stem from an entirely different mechanism being operative in polar solvents with R_3SiCF_3 in reactions with **1**, especially in light of the fact that any open coordination site (as, e.g., required in the PPh_3 exchange outlined above in Figure 5B) would be quenched by the coordinating solvent. To this end, we hypothesized and explored whether an alternative mechanism might be possible in which (partial) fluoride abstraction by R_3SiCF_3 occurs, which would resemble a mechanism that is of greater ionic character and hence potentially more favored in polar solvents.

As the location and energetic evaluation of ionic species with static DFT calculations is associated with challenges,[37] we set out to identify a potential reaction pathway with dynamic calculations of the entire reaction pathway. Recently, Grimme and co-workers have developed a rapid semi-empirical (tight binding) quantum chemical method that is capable to dynamically study systems up to 1000 atoms and implemented it in the xTB package.[38] The main advantage of this approach is the improved computational speed. For comparison, to calculate the single-point energy of the system $[(PPh_3)_2Pd^{(II)}(Ph)(F)]$

https://doi.org/10.1021/jacsau.3c00724
JACS Au 2024, 4, 263−275

and Me_3SiCF_3 embedded in 50 MeCN molecules using Intel Broadwell EP CPU with four cores takes several days at DFT level of theory [i.e., B3LYP-D3/6-31G(d,p), SDD(Pd)], whereas xTB uses only a few seconds. As such, with xTB the entire reaction path can, in principle, be explored (rather than only the trajectory from the transition state as above), and hence, this program can be used for the discovery of reaction mechanisms. However, given the cost-efficient computational methodology, an accurate reflection of absolute energies or a quantitative reproduction of experiment is likely not feasible; qualitative trends are nevertheless within reach and of value in the context of our study. Recently, it also found application in the study of post-TS bifurcation events.[39]

We therefore next embarked on studying the entire transmetalation event in polar solvent using Grimme's xTB approach. To this end, we embedded starting complex *trans*-$[(PPh_3)_2Pd^{(II)}(F)(Ph)]$ **1** and Me_3SiCF_3 in 50 acetonitrile molecules. We used MeCN instead of PhCN (for reasons of computational cost) and subsequently calculated 50 trajectories with xTB molecular dynamics (at 400 K, NVT ensemble; see the SI for the precise simulation parameters). Interestingly, instead of phosphine ligand dissociation from the bisphosphine $Pd^{(II)}$ complex, followed by transmetalation via TS_{TM}, we observed that the phosphines remain fully bound to Pd in the 50 trajectories that we ran. Instead, one trajectory led to the abstraction of the fluoride of $[L_2(Ph)Pd^{(II)}F]$ by Me_3SiCF_3 which is assisted by a molecule of solvent (MeCN), illustrated in Figure 7 (TS_F) (and movie S3), and overall results in the generation of the ion pair $[(PPh_3)_2Pd^{(IIr)}(Ph)(MeCN)]^+$ $[CF_3{-}SiR_3\text{-}F]^-$ (**Int I**).[40,41] Interestingly, when we performed the analogous simulations in benzene instead of MeCN, we were able to observe only significant elongation of the Pd-PPh_3 bond (details in the SI), but no fluoride abstraction, which would be consistent with the above discussion of mechanistic divergence.

We subsequently performed xTB molecular dynamics also on the latter ion pair that we obtained in polar solvent (embedded in 50 MeCN molecules, at 400 K, NVT ensemble) and observed the release of CF_3 anion from $[CF_3{-}SiR_3\text{-}F]^-$, illustrated in Figure 7 (TS_{rb}). We then calculated 500 molecular dynamics trajectories from the DFT-optimized transition state TS_{rb} (at 300 K, NVT ensemble). For 495 of these 500 trajectories, we observed the release of the CF_3 anion from $[CF_3{-}SiR_3\text{-}F]^-$ during the initial 2 ps of simulation. The CF_3 anion then remained configurationally stable in the simulation and did not fragment further to a difluorocarbene.[42] Ultimately, upon rotation, it recombined with the solvent-coordinated $[(PPh_3)_2Pd^{(II)}(MeCN)(Ph)]^+$ cation to give a transient pentavalent $Pd^{(II)}$ species (**II**; in 347 (69%) of the trajectories). The "lifetime" of this transient species was estimated to be between 0.5 and 3.5 ps in the various simulations. Depending on the collapse of this species (**II**) which expels solvent or ligand, the *trans*- or *cis*-$[(PPh_3)_2Pd^{(II)}(CF_3)(Ph)]$ results. (In the other 148 trajectories (30%), the CF_3 anion remained at a roaming stage within 8 ps).

We observed the formation of *trans*-**2** for 86 of the 347 trajectories (17%; path A, Movie S4), while 159 of the 347 trajectories (32%; path B, Movie S5) resulted in *cis*−solvent complex **3** and 102 of the 347 trajectories (20%; path C, Movie S6) gave *cis*-**2**. Overall, the distribution of *cis*/*trans* is 75:25 in the trajectory calculations, which is in agreement with the observed *cis*-preference in the polar/coordinating solvent. This result was also reproduced with DFT-based BOMD in ORCA (100 trajectories, 300 K, NVT ensemble, with only a single explicit PhCN solvent molecule), resulting in a 76:24 ratio of *cis*:*trans* (for details see the SI).

To get an idea of the approximate energies associated with these reactive events, we also performed quantum mechanical searches of key stationary points (Figure 7). The formation of ion pair **Int I** consisting of $[(PPh_3)_2Pd^{(II)}(Ph)(PhCN)]^+$ $[CF_3{-}SiMe_3\text{-}F]^-$ is calculated to require an activation free-energy barrier of only $\Delta G^{\ddagger}$ = 19.3 kcal/mol.[43] From the intermediate ion pair, a CF_3 anion is then released from $[CF_3{-}SiR_3\text{-}F]^-$. The activation free-energy barrier, TS_{rb}, for the process is $\Delta G^{\ddagger}$ = 4.4 kcal/mol relative to the preceding intermediate (and $\Delta G^{\ddagger}$ = 20.7 kcal/mol overall).[44]

The TS_{rb}-generated "free" CF_3 anion then recombines with cationic $Pd^{(II)}$. However, all our attempts to locate the resulting pentavalent species **II** seen in the dynamics also with static DFT, unsurprisingly, led to its collapse. However, using DFT-based BOMD in the gas phase, starting from TS_{rb} (using ORCA, 100 trajectories, NVT ensemble, at 300 K, with one explicit PhCN solvent molecule present), trajectories also proceeded through the transient pentavalent species, and so did higher-level IRC calculations starting at TS_{rb}. As such, both gas-phase DFT-based and explicit solvent xTB-based dynamics reveal analogous reactive events, which are not identifiable through static DFT calculations of stationary points. Consequently, also in the current scenario post-transition-state dynamic effects influence whether *trans*- or the *cis*-$[(PPh_3)_2Pd^{(II)}(CF_3)(Ph)]$ **2** is generated.[45]

Our calculations also show that this CF_3-anion release via TS_F as the key transition state is only favored in polar/coordinating solvent, as our calculation of the same process in the nonpolar solvent benzene gave a barrier $\Delta G^{\ddagger}$ = 35.1 kcal/mol for TS_F, which is higher than the difluorocarbene releasing path via TS_{TM}. This suggests that the fluoride abstraction pathway is unlikely in benzene, in line with the different reaction speeds (and selectivities) seen in polar/coordinating versus nonpolar solvents.

3. SUMMARY AND CONCLUSIONS

Our systematic experimental study of the trifluoromethylation of *trans*-$[(PPh_3)_2Pd^{(II)}(F)(Ph)]$ **1** in different solvents revealed that mixtures of *cis*- and *trans*-$Pd^{(II)}CF_3$ species are formed at room temperature when R_3SiCF_3 is employed. The polar coordinating solvents (PhCN, DMF) lead to predominantly *cis*- and noncoordinating solvents (benzene) to majorly *trans*-$Pd^{(II)}CF_3$. By contrast, when free difluorocarbene is used, only *trans*-$Pd^{(II)}CF_3$ is generated, regardless of the solvent. Our experimental studies showed that *cis*/*trans* isomerization does not take place at room temperature for the polar/coordinating solvents as a consequence of a phosphine ligand being liberated through exchange with a solvent molecule in the *cis*-$Pd^{(II)}CF_3$, which in turn causes inhibition of the isomerization due to the free PPh_3. In benzene, the *cis*/*trans* isomerization can occur. A statistically representative number of trajectory calculations of the bond-making and -breaking events revealed that different mechanisms are likely undergone. In nonpolar reaction medium, Born−Oppenheimer molecular dynamics simulations suggest that a difluorocarbene is liberated in the transmetalation of $Pd^{(II)}$-F with R_3SiCF_3. The difluorocarbene subsequently *roams* and either directly inserts into $Pd^{(II)}$-F (ultimately leading to the *cis* geometry) or initially binds to $Pd^{(II)}$, followed by a 1,2-F shift (leading to *trans*). As such, a single transmetalation TS (and difluorocarbene release) can give rise to both the *cis*- and *trans* $Pd^{(II)}$ intermediates directly through post-TS bifurcation, which

https://doi.org/10.1021/jacsau.3c00724
JACS Au 2024, 4, 263−275

is not usually considered in reactivity analyses of organometallic transformations. The fate of the *cis*/*trans* distribution of generated $[L_nPd^{(II)}(CF_3)(Ph)]$ is dependent on the phosphine ligand and ligation state.

Through the use of Grimme's xTB program, which allowed us to perform 500 trajectory calculations with explicit MeCN solvation, we found that for polar (and coordinating) solvents a zwitterionic mechanism is likely favored. The transmetalating agent Me_3SiCF_3 initially abstracts a fluoride anion to form the ion pair $[(PPh_3)_2Pd^{(II)}(Ph)(MeCN)]^+$ $[CF_3{-}SiR_3\text{-}F]^-$ from which a CF_3 anion is subsequently expelled, which then roams and rebinds to the $Pd^{(II)}$ cation to form the *trans*- or *cis*-product, respectively. Again, post-transition-state dynamic effects led to both possible intermediates directly.

This study manifests the value of dynamic calculations to reveal mechanisms and post-transition-state reactive events and constitutes the first identification of a post-transition-state dynamic reactivity effect (bifurcation) in the widely employed Pd-catalyzed cross-coupling class.

4. METHODS

4.1. Experimental Details

All reactions were performed under inert conditions inside an argon-filled glovebox, unless otherwise noted. All reagents were purchased from Sigma-Aldrich, TCI, or ABCR except for silver fluoride, which was purchased from FluoroChem. Complex $[(PPh_3)_2Pd(C_6H_5)F]$ **1**,[19] $[(tmeda)Pd(Ph)CF_3]$,[23] and $PPh_3CF_2CO_2$[19] were synthesized according to known procedures. Reagents were used as received, unless noted otherwise. Only anhydrous solvents were used and either purchased from Aldrich or purified using a solvent drying system from Innovative Technology Pure Solvent PS-MD-5 under an argon atmosphere.

All ^{1}H NMR, ^{13}C NMR and ^{19}F NMR, and ^{31}P NMR spectra were recorded at ambient temperature on Bruker Avance Neo 600, Varian V-NMRS 600, or Varian V-NMRS 400 spectrometers. Chemical shifts are reported in parts per million, relative to solvent residual peaks or internally by the instrument after locking and shimming to the deuterated solvent (for ^{19}F). Quantitative ^{19}F NMR spectra were recorded using 10 s relaxation delay, 90° pulse angle, and 16−32 scans. High-resolution mass spectrometry (HRMS) was performed using a Bruker Maxis II LC-MS-System (APCI). IR spectra were measured on a PerkinElmer Spectrum 100 FT-IR using the universal ATR (UATR) accessory.

4.1.1. Transmetalation with In Situ-Generated Difluorocarbene (Figure 2, Top). In the glovebox, **1** (36.3 mg, 0.05 mmol, 1.0 equiv) and $[PPh_3CF_2CO_2]$ (26.7 mg, 0.075 mmol, 1.5 equiv) were added into an oven-dried scintillation vial (4 mL) and dissolved in 1 mL of anhydrous solvent (DCM, C_6H_6, or DMF). The reactions were allowed to stir at room temperature, and the yield of *cis*-2 and/or *trans*-2 was determined by quantitative ^{19}F NMR analysis after 1 h (for DCM) or 24 h (for C_6H_6, DMF).

4.1.2. Transmetalation with Et_3SiCF_3 (Figure 2, Bottom). In the glovebox, in a scintillation vial (4 mL), a stock solution of Et_3SiCF_3 (5 μL, 27.69 μmol) and internal standard (4,4′-difluorobiphenyl) in a given solvent (1.5 mL) was prepared. An NMR tube was then charged with **1** (ca. 5.5 μmol, 1.0 equiv) and sealed with a rubber septum and parafilm. The stock solution (0.75 mL) was then added to the NMR tube via a syringe directly before starting the quantitative ^{19}F NMR analysis.

4.1.3. Synthesis of *Cis*-$[(PPh_3)_2Pd^{(II)}(CF_3)(Ph)]$ (*Cis*-2, Figure 3A). In the glovebox, $[(tmeda)Pd(Ph)CF_3]$ (150 mg, 0.4 mmol, 1 equiv), PPh_3 (470 mg, 1.8 mmol, 4.5 equiv), and $KHSO_4$ (800 mg) were dissolved in DCM (5 mL) in a 20 mL vial. The vial was sealed with a screw cap and was taken out of the glovebox and stirred at room temperature for 12 h with all further manipulations performed open to air. After the stated time, the reaction was filtered through cotton and a plug (ca. 2 cm in a glass pipette) of Na_2SO_4. The reaction was then concentrated to ca. 1 M before double the volume of 1:1 Et_2O/pentane was added, causing instant crystallization. The solid was then rinsed with 1:1 Et_2O/pentane to yield *cis*-**2** (272 mg, 0.35 mmol, 87%). CCDC 2172315 contains the supporting crystallographic data for this compound. **^{1}H NMR** (600 MHz, methylene chloride-d_2): δ 7.34 (ddd, J = 10.1, 8.1, 1.3 Hz, 6H), 7.30 (ddd, J = 7.4, 7.4, 1.6 Hz, 3H), 7.26−7.20 (m, 11H), 7.18 (ddd, J = 7.8, 7.7, 2.0 Hz, 6H), 7.07 (ddd, J = 8.0, 7.8, 2.1 Hz, 6H), 6.60 (ddd, J = 7.7, 7.4, 2.0 Hz, 2H), 6.54 (dd, J = 7.1, 7.1 Hz, 1H). **^{19}F NMR** (565 MHz, methylene chloride-d_2): δ −18.77 (dd, J = 45.7, 15.0 Hz, 3F). **^{31}P NMR** (243 MHz, methylene chloride-d_2): δ 25.72 (qd, J = 46.3, 26.2 Hz, 1P), 21.14 (dq, J = 25.6, 14.9 Hz, 1P). **IR** (neat, cm^{-1}): 3050, 1562, 1478, 1433. **HRMS** (APCI): calculated $C_{37}H_{30}F_3P_2Pd$ $[M\text{-}Ph]^+$: 699.0818, found 699.0841.

4.1.4. Synthesis of *Cis*-$[(PPh_3)(MeCN)Pd^{(II)}(CF_3)(Ph)]$ (*Cis*-3, Figure 3A). Under inert atmosphere, $[(tmeda)Pd(Ph)CF_3]$ (200 mg, 0.54 mmol, 1 equiv) and $KHSO_4$ (5 g) were dissolved in MeCN (15 mL) and stirred at room temperature for 5 h. After the stated time, the reaction was filtered through a plug of Na_2SO_4 and washed with DCM (3 × 10 mL). The reaction was then concentrated to ca. 2 mL before being diluted with DCM and reduced to ca. 2 mL again. To this was added PPh_3 (142.0 mg, 0.54 mmol, 1 equiv) in DCM (15 mL) and stirred for 2 min. After this time, the reaction was concentrated to ca. 1 mL and filtered by a syringe filter to yield a yellow solution. The title compound could be obtained by recrystallization by layering with 40% diethyl ether in pentane (85.3 mg, 0.15 mmol, 28%). *Note:* In solution, it was found that the compound was unstable to light/heat, leading to deposition of Pd black and degradation of purity. CCDC 2172314 contains the supplementary crystallographic data for this compound. **^{1}H NMR** (600 MHz, methylene chloride-d_2): δ 7.41 (ddd, J = 7.3, 1.6 Hz, 3H), 7.33 (ddd, J = 7.8, 2.2 Hz, 6H), 7.30−7.25 (m, 6H), 7.06 (d, J = 7.2 Hz, 2H), 6.74−6.67 (m, 3H), 1.70 (s, 3H). **^{19}F NMR** (565 MHz, methylene chloride-d_2): δ −25.42 (d, J = 46.4 Hz). **^{31}P NMR** (243 MHz, methylene chloride-d_2): δ 18.97 (dddt, J = 56.3, 45.6, 34.4, 10.6 Hz). **IR** (neat, cm^{-1}): 3653, 3059, 1567, 1478, 1434. **HRMS** (APCI): calculated for $C_{21}H_{18}F_3PNPd$ $[M\text{-}Ph]^+$: 478.0167, found 478.0168.

4.1.5. *Cis*−*Trans* Isomerization of Cis-2 in Presence or Absence of PPh_3 (Figure 3B). In the glovebox, into an NMR tube was weighed *cis*-**2** (4.2 mg, 0.005 mmol, 1 equiv), PPh_3 (3.8 mg, 0.015 mmol, 2.5 equiv), and 4,4′-difluorobiphenyl (as an internal standard). In one portion was added 0.75 mL of C_6D_6, and the reaction mixture was immediately transferred to a preheated NMR machine at 50 °C. The isomerization was monitored by quantitative ^{19}F NMR spectroscopy.

4.2. Computational Methods

All static DFT calculations were performed with the Gaussian 09 program package (revision D.01).[28] Gas-phase structural optimizations and frequency calculations were performed with B3LYP[46]-D3 along with 6-31G(d,p)[47] basis set on C, H, F, P, and Si atoms, and the effective core potential (ECP) SDD[48] on Pd. D3 corrections were applied using the original D3 damping functions proposed by Grimme and co-workers.[49] Single-point energy calculations were performed with M06L[50] and def2-TZVP[51] basis sets. Solvation energies were described using the SMD[52] model (for benzene of benzonitrile). Frequency calculations were performed to confirm whether the structure is a minimum or a transition state. Intrinsic reaction coordinate (IRC) analysis was used to confirm that the obtained transition states connect the corresponding reactants and products.

Molecular dynamics calculations at the DFT level (Born−Oppenheimer molecular dynamics, BOMD) were performed at the B3LYP-D3/6-31G(d)(SDD on Pd) level of theory in the gas phase using either Gaussian 09, revision D.01,[28] or ORCA 5.0.3.[32] BOMD calculations using Gaussian ("BOMD" keyword) were run as a microcanonical ensemble (NVE), i.e., under conservation of total energy. The calculations were run at a temperature of 300 K, implemented through the initial kinetic energy ("nke" keyword) as $\text{nke} = (\text{numberofatoms} - 1)\frac{3}{2}kT$, where k is Boltzmann's constant and T is the temperature. A step size of 1 fs was used, and initial velocities were generated through a random number seed ("random-velocity" keyword). BOMD calculations in the ORCA were run as a canonical ensemble (NVT), i.e., at a constant temperature of 300 K,

https://doi.org/10.1021/jacsau.3c00724
JACS Au 2024, 4, 263−275

implemented through the Berendsen thermostat and using a step size of 0.5 fs. Initial velocities were generated through a random number seed (using the "Randomize" keyword).

Molecular dynamics calculations in solvent were performed using xtb 6.5.1 with GFN2-xTB.[38] Explicit solvent molecules (30 benzene or 50 acetonitrile molecules) were placed randomly around the solute and preoptimized (only optimizing the solvent while fixing the solute) before molecular dynamics calculations. To avoid solvent dissociation, the explored systems were confined within a ball with radii according to the density of the employed solvent (using "logfermi" potential). xTB-MD calculations were run as a canonical ensemble (NVT) using the Berendsen thermostat at either 300 K (when starting from a transition state) or 400 K (when starting from reactants; to facilitate reactivity). The mass of all hydrogen atoms was set to 4 (default settings) to allow for a larger time step size of 2 fs.

■ ASSOCIATED CONTENT

Supporting Information

The Supporting Information is available free of charge at https://pubs.acs.org/doi/10.1021/jacsau.3c00724.

Non-polar_trans (Movie S1) (MP4)
Non-polar_cis (Movie S2) (MP4)
Polar_F-abstraction (Movie S3) (MP4)
Polar_trans (Movie S4) (MP4)
Polar_cis (Movie S5) (MP4)
Experimental information and procedures; crystallographic details; computational details; NMR spectra; and movies of representative trajectories (PDF)
Polar_cis-2 (Movie S6) (MP4)

■ AUTHOR INFORMATION

Corresponding Author

Franziska Schoenebeck − *Institute of Organic Chemistry, RWTH Aachen University, 52074 Aachen, Germany;* orcid.org/0000-0003-0047-0929; Email: franziska.schoenebeck@rwth-aachen.de

Authors

Maoping Pu − *Institute of Organic Chemistry, RWTH Aachen University, 52074 Aachen, Germany*

Christian D.-T. Nielsen − *Institute of Organic Chemistry, RWTH Aachen University, 52074 Aachen, Germany*

Erdem Senol − *Institute of Organic Chemistry, RWTH Aachen University, 52074 Aachen, Germany*

Theresa Sperger − *Institute of Organic Chemistry, RWTH Aachen University, 52074 Aachen, Germany;* orcid.org/0000-0002-3870-9870

Complete contact information is available at: https://pubs.acs.org/10.1021/jacsau.3c00724

Author Contributions

CRediT: **Maoping Pu** data curation, formal analysis, investigation; **Christian Nielsen** data curation, formal analysis; **Erdem Senol** data curation, formal analysis; **Franziska Schoenebeck** conceptualization, formal analysis, funding acquisition.

Notes

The authors declare no competing financial interest.

■ ACKNOWLEDGMENTS

The authors thank the European Research Council for the funding. Calculations were performed with computing resources granted by JARA-HPC from RWTH Aachen University under project "jara0091".

■ REFERENCES

(1) (a) Yang, Z.; Jamieson, C. S.; Xue, X.-S.; Garcia-Borràs, M.; Benton, T.; Dong, X.; Liu, F.; Houk, K. N. Mechanisms and Dynamics of Reactions Involving Entropic Intermediates. *Trends Chem.* **2019**, *1*, 22−34. (b) Yang, Z. Y.; Houk, K. N. The Dynamics of Chemical Reactions: Atomistic Visualizations of Organic Reactions, and Homage to van 't Hoff. *Chem. − Eur. J.* **2018**, *24*, 3916−3924. (c) Tantillo, D. J. Questions in natural products synthesis research that can (and cannot) be answered using computational chemistry. *Chem. Soc. Rev.* **2018**, *47*, 7845−7850. (d) Hare, S. R.; Tantillo, D. J. Post-Transition State Bifurcations Gain Momentum - Current State of the Field. *Pure Appl. Chem.* **2017**, *89*, 679−698. (e) Rehbein, J.; Wulff, B. Chemistry in motion-off the MEP. *Tetrahedron Lett.* **2015**, *56*, 6931−6943. (f) Carpenter, B. K. Energy Disposition in Reactive Intermediates. *Chem. Rev.* **2013**, *113*, 7265−7286. (g) Carpenter, B. K. Nonstatistical Dynamics in Thermal Reactions of Polyatomic Molecules. *Annu. Rev. Phys. Chem.* **2005**, *56*, 57−89. (h) Carpenter, B. K. Intramolecular Dynamics for the Organic Chemist. *Acc. Chem. Res.* **1992**, *25*, 520−528. (i) Ess, D. H.; Wheeler, S. E.; Iafe, R. G.; Xu, L.; Celebi-Olcum, N.; Houk, K. N. Bifurcations on Potential Energy Surfaces of Organic Reactions. *Angew. Chem., Int. Ed.* **2008**, *47*, 7592−7601. (j) Mikosch, J.; Trippel, S.; Eichhorn, C.; Otto, R.; Lourderaj, U.; Zhang, J. X.; Hase, W. L.; Weidemuller, M.; Wester, R. Imaging nucleophilic substitution dynamics. *Science* **2008**, *319*, 183−186. (k) Ammal, S. C.; Yamataka, H.; Aida, M.; Dupuis, M. Dynamics-driven reaction pathway in an intramolecular rearrangement. *Science* **2003**, *299*, 1555−1557. (l) Sun, L. P.; Song, K. Y.; Hase, W. L. A S_N2 reaction that avoids its deep potential energy minimum. *Science* **2002**, *296*, 875−878.

(2) (a) Townsend, D.; Lahankar, S. A.; Lee, S. K.; Chambreau, S. D.; Suits, A. G.; Zhang, X.; Rheinecker, J.; Harding, L. B.; Bowman, J. M. The roaming atom: Straying from the reaction path in formaldehyde decomposition. *Science* **2004**, *306*, 1158−1161. (b) Collins, P.; Kramer, Z. C.; Carpenter, B. K.; Ezra, G. S.; Wiggins, S. Nonstatistical dynamics on the caldera. *J. Chem. Phys.* **2014**, *141*, No. 034111. (c) Doering, W. v. E.; Barsa, E. A. Fate of Diradicals in the Caldera: Stereochemistry of Thermal Stereomutation and Ring Enlargement in cis- and trans-1-Cyano-2(*E*)-propenylcyclopropanes. *J. Am. Chem. Soc.* **2004**, *126*, 12353−12362. (d) Doering, W. v. E.; Cheng, X.; Lee, K.; Lin, Z. Fate of the Intermediate Diradicals in the Caldera: Stereochemistry of Thermal Stereomutations, (2 + 2) Cycloreversions, and (2 + 4) Ring-Enlargements of cis- and trans-1-Cyano-2-(E and Z)-propenyl-cis-3,4-dideuteriocyclobutanes. *J. Am. Chem. Soc.* **2002**, *124*, 11642−11652.

(3) Yang, Z. Y.; Dong, X. F.; Yu, Y. M.; Yu, P. Y.; Li, Y. Z.; Jamieson, C.; Houk, K. N. Relationships between Product Ratios in Ambimodal Pericyclic Reactions and Bond Lengths in Transition Structures. *J. Am. Chem. Soc.* **2018**, *140*, 3061−3067.

(4) (a) Popov, S.; Shao, B.; Bagdasarian, A. L.; Benton, T. R.; Zou, L. Y.; Yang, Z. Y.; Houk, K. N.; Nelson, H. M. Teaching an old carbocation new tricks: Intermolecular C-H insertion reactions of vinyl cations. *Science* **2018**, *361*, 381−387. (b) Blümel, M.; Nagasawa, S.; Blackford, K.; Hare, S. R.; Tantillo, D. J.; Sarpong, R. Rearrangement of Hydroxylated Pinene Derivatives to Fenchone Type Frameworks: Computational Evidence for Dynamically-Controlled Selectivity. *J. Am. Chem. Soc.* **2018**, *140*, 9291−9298. (c) Zheng, C.; Xia, Z. L.; You, S. L. Unified Mechanistic Understandings of Pictet-Spengler Reactions. *Chem* **2018**, *4*, 1952−1966. (d) Chen, S.; Yu, P.; Houk, K. N. Ambimodal Dipolar/Diels−Alder Cycloaddition Transition States Involving Proton Transfers. *J. Am. Chem. Soc.* **2018**, *140*, 18124−18131. (e) Tan, J. S. J.; Hirvonen, V.; Paton, R. S. Dynamic Intermediates in the Radical Cation Diels-Alder Cycloaddition: Lifetime and Suprafacial Stereoselectivity. *Org. Lett.* **2018**, *20*, 2821−2825. (f) Hare, S. R.; Pemberton, R. P.; Tantillo, D. J. Navigating Past a Fork in the Road: Carbocation-p Interactions Can Manipulate Dynamic Behavior of Reactions Facing Post-Transition-State Bifurcations. *J. Am. Chem. Soc.* **2017**, *139*, 7485−7493. (g) Yu, P. Y.; Chen, T.

Q.; Yang, Z. Y.; He, C. Q.; Patel, A.; Lam, Y. H.; Liu, C. Y.; Houk, K. N. Mechanisms and Origins of Periselectivity of the Ambimodal [6 + 4] Cycloadditions of Tropone to Dimethylfulvene. *J. Am. Chem. Soc.* **2017**, *139*, 8251−8258. (h) Feng, Z.; Tantillo, D. J. Dynamic Effects on Migratory Aptitudes in Carbocation Reactions. *J. Am. Chem. Soc.* **2021**, *143*, 1088−1097. (i) Xue, X.-S.; Jamieson, C. S.; Garcia-Borràs, M.; Dong, X.; Yang, Z.; Houk, K. N. Ambimodal Trispericyclic Transition State and Dynamic Control of Periselectivity. *J. Am. Chem. Soc.* **2019**, *141*, 1217−1221.

(5) (a) Yang, Z. Y.; Yang, S.; Yu, P. Y.; Li, Y. W.; Doubleday, C.; Park, J.; Patel, A.; Jeon, B. S.; Russell, W. K.; Liu, H. W.; Russell, D. H.; Houk, K. N. Influence of water and enzyme SpnF on the dynamics and energetics of the ambimodal [6 + 4]/[4 + 2] cycloaddition. *Proc. Natl. Acad. Sci. U.S.A.* **2018**, *115*, E848−E855. (b) Ohashi, M.; Liu, F.; Hai, Y.; Chen, M. B.; Tang, M. C.; Yang, Z. Y.; Sato, M.; Watanabe, K.; Houk, K. N.; Tang, Y. SAM-dependent enzyme-catalysed pericyclic reactions in natural product biosynthesis. *Nature* **2017**, *549*, 502−508. (c) Hong, Y. J.; Tantillo, D. J. Biosynthetic Consequences of Multiple sequential Post-Transition-State Bifurcations. *Nat. Chem.* **2014**, *6*, 104−111.

(6) (a) Ess, D. H. Quasiclassical Direct Dynamics Trajectory Simulations of Organometallic Reactions. *Acc. Chem. Res.* **2021**, *54*, 4410−4422. (b) Hansen, J. H.; Gregg, T. M.; Ovalles, S. R.; Lian, Y. J.; Autschbach, J.; Davies, H. M. L. On the Mechanism and Selectivity of the Combined C-H Activation/Cope Rearrangement. *J. Am. Chem. Soc.* **2011**, *133*, 5076−5085. (c) Hansmann, M. M.; Rudolph, M.; Rominger, F.; Hashmi, A. S. K. Mechanistic Switch in Dual Gold Catalysis of Diynes: C(sp^3)-H Activation through Bifurcation-Vinylidene versus Carbene Pathways. *Angew. Chem., Int. Ed.* **2013**, *52*, 2593−2598. (d) Noey, E. L.; Wang, X.; Houk, K. N. Selective Gold(I)-Catalyzed Formation of Tetracyclic Indolines: A Single Transition Structure and Bifurcations Lead to Multiple Products. *J. Org. Chem.* **2011**, *76*, 3477−3483. (e) Hare, S. R.; Tantillo, D. J. Cryptic Post-Transition State Bifurcations That Reduce the Efficiency of Lactone-forming Rh-carbenoid C-H Insertions. *Chem. Sci.* **2017**, *8*, 1442−1449. (f) Ye, L. W.; Wang, Y. Z.; Aue, D. H.; Zhang, L. M. Experimental and Computational Evidence for Gold Vinylidenes: Generation from Terminal Alkynes via a Bifurcation Pathway and Facile C-H Insertions. *J. Am. Chem. Soc.* **2012**, *134*, 31−34. (g) Yang, B.; Schouten, A.; Ess, D. H. Direct Dynamics Trajectories Reveal Nonstatistical Coordination Intermediates and Demonstrate that σ and π-Coordination Are Not Required for Rhenium(I)-Mediated Ethylene C−H Activation. *J. Am. Chem. Soc.* **2021**, *143*, 8367−8374. (h) Kpante, M.; Wolf, L. M. Pathway Bifurcations in the Activation of Allylic Halides by Palladium and Their Influence on the Dynamics of η^1 and η^3 Allyl Intermediates. *J. Org. Chem.* **2021**, *86*, 9637−9650.

(7) *Handbook of Organopalladium Chemistry for Organic Synthesis*; Negishi, E.-i.; De Meijere, A., Eds.; John Wiley & Sons: New York, 2002; Vol. *2*.

(8) (a) García-Melchor, M.; Braga, A. A. C.; Lledos, A.; Ujaque, G.; Maseras, F. Computational Perspective on Pd-Catalyzed C-C Cross-Coupling Reaction Mechanisms. *Acc. Chem. Res.* **2013**, *46*, 2626−2634. (b) Thomas, A. A.; Denmark, S. E. Pre-transmetalation intermediates in the Suzuki-Miyaura reaction revealed: The missing link. *Science* **2016**, *352*, 329−332. (c) del Pozo, J.; Salas, G.; Alvarez, R.; Casares, J. A.; Espinet, P. The Negishi Catalysis: Full Study of the Complications in the Transmetalation Step and Consequences for the Coupling Products. *Organometallics* **2016**, *35*, 3604−3611. (d) Espinet, P.; Echavarren, A. M. The Mechanisms of the Stille Reaction. *Angew. Chem., Int. Ed.* **2004**, *43*, 4704−4734. (e) Hiyama, T. How I Came Across the Silicon-based Cross-coupling Reaction. *J. Organomet. Chem.* **2002**, *653*, 58−61. (f) Miyaura, N.; Suzuki, A. Palladium-Catalyzed Cross-Coupling Reactions of Organoboron Compounds. *Chem. Rev.* **1995**, *95*, 2457−2483.

(9) Cho, E. J.; Senecal, T. D.; Kinzel, T.; Zhang, Y.; Watson, D. A.; Buchwald, S. L. The palladium-catalyzed trifluoromethylation of aryl chlorides. *Science* **2010**, *328*, 1679−1681.

(10) Ferguson, D. M.; Bour, J. R.; Canty, A. J.; Kampf, J. W.; Sanford, M. S. Stoichiometric and Catalytic Aryl-Perfluoroalkyl Coupling at Tri-*tert*-butylphosphine Palladium(II) Complexes. *J. Am. Chem. Soc.* **2017**, *139*, 11662−11665. With bulkly monophosphine Pd species, no high yields were achieved and challenging side reactions shown. See:

(11) Keaveney, S. T.; Schoenebeck, F. Palladium-Catalyzed Decarbonylative Trifluoromethylation of Acid Fluorides. *Angew. Chem., Int. Ed.* **2018**, *57*, 4073−4077.

(12) (a) Liang, T.; Neumann, C. N.; Ritter, T. Introduction of Fluorine and Fluorine-Containing Functional Groups. *Angew. Chem., Int. Ed.* **2013**, *52*, 8214−8264. (b) Berger, R.; Resnati, G.; Metrangolo, P.; Weber, E.; Hulliger, J. Organic fluorine compounds: a great opportunity for enhanced materials properties. *Chem. Soc. Rev.* **2011**, *40*, 3496−3508. (c) Purser, S.; Moore, P. R.; Swallow, S.; Gouverneur, V. Fluorine in medicinal chemistry. *Chem. Soc. Rev.* **2008**, *37*, 320−330.

(13) Tomashenko, O. A.; Grushin, V. V. Aromatic Trifluoromethylation with Metal Complexes. *Chem. Rev.* **2011**, *111*, 4475−4521.

(14) García-Domínguez, A.; West, T. H.; Primozic, J. J.; Grant, K. M.; Johnston, C. P.; Cumming, G. G.; Leach, A. G.; Lloyd-Jones, G. C. Difluorocarbene Generation from $TMSCF_3$: Kinetics and Mechanism of NaI-Mediated and Si-Induced Anionic Chain Reactions. *J. Am. Chem. Soc.* **2020**, *142*, 14649−14663.

(15) (a) Grushin, V. V.; Marshall, W. J. Facile Ar−CF_3 Bond Formation at Pd. Strikingly Different Outcomes of Reductive Elimination from $[(Ph_3P)_2Pd(CF_3)Ph]$ and [(Xantphos)Pd(CF_3)Ph]. *J. Am. Chem. Soc.* **2006**, *128*, 12644−12645. (b) Bakhmutov, V. I.; Bozoglian, F.; Gómez, K.; González, G.; Grushin, V. V.; Macgregor, S. A.; Martin, E.; Miloserdov, F. M.; Novikov, M. A.; Panetier, J. A.; Romashov, L. V. CF_3−Ph Reductive Elimination from [(Xantphos)-Pd(CF_3)(Ph)]. *Organometallics* **2012**, *31*, 1315−1328.

(16) (a) Ferguson, D. M.; Bour, J. R.; Canty, A. J.; Kampf, J. W.; Sanford, M. S. Stoichiometric and Catalytic Aryl-Perfluoroalkyl Coupling at Tri-*tert*-butylphosphine Palladium(II) Complexes. *J. Am. Chem. Soc.* **2017**, *139*, 11662−11665. (b) Nielsen, M. C.; Bonney, K. J.; Schoenebeck, F. Computational Ligand Design for the Reductive Elimination of $ArCF_3$ from a Small Bite Angle Pd^{II} Complex: Remarkable Effect of a Perfluoroalkyl Phosphine. *Angew. Chem., Int. Ed.* **2014**, *53*, 5903−5906.

(17) For reviews, see: (a) Ogiwara, Y.; Sakai, N. Acyl Fluorides in Late-Transition-Metal Catalysis. *Angew. Chem., Int. Ed.* **2020**, *59*, 574−594. (b) Lalloo, N.; Brigham, C. E.; Sanford, M. S. Mechanism-Driven Development of Group 10 Metal-Catalyzed Decarbonylative Coupling Reactions. *Acc. Chem. Res.* **2022**, *55*, 3430−3444.

(18) Lalloo, N.; Malapit, C. A.; Taimoory, S. M.; Brigham, C. E.; Sanford, M. S. Decarbonylative Fluoroalkylation at Palladium(II): From Fundamental Organometallic Studies to Catalysis. *J. Am. Chem. Soc.* **2021**, *143*, 18617−18625.

(19) Pu, M.; Sanhueza, I. A.; Senol, E.; Schoenebeck, F. Divergent Reactivity of Stannane and Silane in the Trifluoromethylation of Pd^{II}: Cyclic Transition State versus Difluorocarbene Release. *Angew. Chem., Int. Ed.* **2018**, *57*, 15081−15085.

(20) (a) Lennox, A. J. J.; Lloyd-Jones, G. C. Transmetalation in the Suzuki-Miyaura Coupling: The Fork in the Trail. *Angew. Chem., Int. Ed.* **2013**, *52*, 7362−7370. (b) Butters, M.; Harvey, J. N.; Jover, J.; Lennox, A. J. J.; Lloyd-Jones, G. C.; Murray, P. M. Aryl Trifluoroborates in Suzuki-Miyaura Coupling: The Roles of Endogenous Aryl Boronic Acid and Fluoride. *Angew. Chem., Int. Ed.* **2010**, *49*, 5156−5160. (c) Amatore, C.; Bahsoun, A. A.; Jutand, A.; Meyer, G.; Ntepe, A. N.; Ricard, L. Mechanism of the Stille reaction catalyzed by palladium ligated to arsine ligand: PhPdI($AsPh_3$)(DMF) is the species reacting with vinylstannane in DMF. *J. Am. Chem. Soc.* **2003**, *125*, 4212−4222.

(21) Pilon, M. C.; Grushin, V. V. Synthesis and Characterization of Organopalladium Complexes Containing a Fluoro Ligand. *Organometallics* **1998**, *17*, 1774−1781. For the first synthesis of this complex, see:

(22) *Cis* and *trans* are not well defined for monophosphine $Pd^{(II)}$ complexes. In this article, *cis* and *trans* refer to the relationship of CF_3 and Ph (see Figure 4).

(23) Grushin, V. V.; Marshall, W. J. Unexpected H_2O-Induced Ar−X Activation with Trifluoromethylpalladium(II) Aryls. *J. Am. Chem. Soc.* **2006**, *128*, 4632−4641.

https://doi.org/10.1021/jacsau.3c00724
JACS Au 2024, 4, 263−275

(24) Deposition numbers 2172315 (for cis-2), and 2172314 (for ***cis-3***) contain the supplementary crystallographic data for this paper. These data are provided free of charge by the joint Cambridge Crystallographic Data Centre and Fachinformationszentrum Karlsruhe Access Structures service.

(25) (a) Grushin, V. V.; Alper, H. Indirect Formation of Carboxylic Acids via Anhydrides in the Palladium-Catalyzed Hydroxycarbonylation of Aromatic Halides. *J. Am. Chem. Soc.* **1995**, *117*, 4305−4315. (b) Normand, A. T.; Nechaev, M. S.; Cavell, K. J. Mechanisms in the Reaction of Palladium(II)−π-Allyl Complexes with Aryl Halides: Evidence for NHC Exchange Between Two Palladium Complexes. *Chem. − Eur. J.* **2009**, *15*, 7063−7073.

(26) (a) Nova, A.; Ujaque, G.; Maseras, F.; Lledós, A.; Espinet, P. A critical analysis of the cyclic and open alternatives of the transmetalation step in the stille cross-coupling reaction. *J. Am. Chem. Soc.* **2006**, *128*, 14571−14578. (b) Grushin, V. V. Thermal Stability, Decomposition Paths, and Ph/Ph Exchange Reactions of $[(Ph_3P)_2Pd(Ph)X]$ (X = I, Br, Cl, F, and HF_2). *Organometallics* **2000**, *19*, 1888−1900.

(27) Wang, L. P.; Titov, A.; McGibbon, R.; Liu, F.; Pande, V. S.; Martinez, T. J. Discovering chemistry with an ab initio nanoreactor. *Nat. Chem.* **2014**, *6*, 1044−1048.

(28) Frisch, M. J.; Trucks, G. W.; Schlegel, H. B.; Scuseria, G. E.; Robb, M. A.; Cheeseman, J. R.; Scalmani, G.; Barone, V.; Mennucci, B.; Petersson, G. A.; Nakatsuji, H.; Caricato, M.; Li, X.; Hratchian, H. P.; Izmaylov, A. F.; Bloino, J.; Zheng, G.; Sonnenberg, J. L.; Hada, M.; Ehara, M.; Toyota, K.; Fukuda, R.; Hasegawa, J.; Ishida, M.; Nakajima, T.; Honda, Y.; Kitao, O.; Nakai, H.; Vreven, T.; Montgomery, J. A., Jr.; Peralta, J. E.; Ogliaro, F.; Bearpark, M.; Heyd, J. J.; Brothers, E.; Kudin, K. N.; Staroverov, V. N.; Keith, T.; Kobayashi, R.; Normand, J.; Raghavachari, K.; Rendell, A.; Burant, J. C.; Iyengar, S. S.; Tomasi, J.; Cossi, M.; Rega, N.; Millam, J. M.; Klene, M.; Knox, J. E.; Cross, J. B.; Bakken, V.; Adamo, C.; Jaramillo, J.; Gomperts, R.; Stratmann, R. E.; Yazyev, O.; Austin, A. J.; Cammi, R.; Pomelli, C.; Ochterski, J. W.; Martin, R. L.; Morokuma, K.; Zakrzewski, V. G.; Voth, G. A.; Salvador, P.; Dannenberg, J. J.; Dapprich, S.; Daniels, A. D.; Farkas, O.; Foresman, J. B.; Ortiz, J. V.; Cioslowski, J.; Fox, D. J. *Gaussian 09*, Revision D.01; Gaussian, Inc.: Wallingford CT, 2013.

(29) Brahms, D. L. S.; Dailey, W. P. Fluorinated Carbenes. *Chem. Rev.* **1996**, *96*, 1585−1632, DOI: 10.1021/cr941141k. Since CF_2 carbene has a singlet ground state (see:no adjustment in overall multiplicity was necessary during the BOMD calculations

(30) Pu, M. P.; Sanhueza, I. A.; Senol, E.; Schoenebeck, F. Divergent Reactivity of Stannane and Silane in the Trifluoromethylation of Pd^{II}: Cyclic Transition State versus Difluorocarbene Release. *Angew. Chem., Int. Ed.* **2018**, *57*, 15081−15085.

(31) Since the total energy is kept constant under NVE (micro-canonical) conditions, this might not be appropriate to represent experimental conditions under which only the kinetic energy (not the potential energy) remains constant. While an NPT ensemble would best represent experimental conditions (requires use of a barostat, which is not easily available), the NVT (canonical) ensemble is a good approximation assuming there are only negligible changes in solvent density and therefore constant pressure equals constant volume. Calculations of an NVT ensemble require a thermostat, which is available in both xTB and ORCA software.

(32) Neese, F. Software update: The ORCA program system−Version 5.0. *Wiley Interdiscip. Rev.: Comput. Mol. Sci.* **2022**, *12*, No. e1606, DOI: 10.1002/wcms.1606.

(33) Pu, M.; Privalov, T. Uncovering the Role of Intra- and Intermolecular Motion in Frustrated Lewis Acid/Base Chemistry: Ab Initio Molecular Dynamics Study of CO_2 Binding by Phosphorus/Boron Frustrated Lewis Pair $[tBu_3P/B(C_6F_5)_3]$. *Inorg. Chem.* **2014**, *53*, 4598−4609. A previous study has also obtained analogous results under NVE and NVT ensembles:

(34) For appropriateness of method, see: Sperger, T.; Sanhueza, I. A.; Kalvet, I.; Schoenebeck, F. Computational Studies of Synthetically Relevant Homogeneous Organometallic Catalysis Involving Ni, Pd, Ir, and Rh: An Overview of Commonly Employed DFT Methods and Mechanistic Insights. *Chem. Rev.* **2015**, *115*, 9532−9586.

(35) Sugiyama, A.; Ohnishi, Y.-y.; Nakaoka, M.; Nakao, Y.; Sato, H.; Sakaki, S.; Nakao, Y.; Hiyama, T. Why Does Fluoride Anion Accelerate Transmetalation between Vinylsilane and Palladium(II)−Vinyl Complex? Theoretical Study. *J. Am. Chem. Soc.* **2008**, *130*, 12975−12985.

(36) The variation of the overall activation free energy barrier to reach TSTM was less pronounced however (when the ligand dissociation energy was larger, smaller subsequent activation barriers were calculated and vice-versa, see SI for further information).

(37) Such challenges include the inability to locate zwitterionic species or ion-pairs as stationary points or potential artifacts in ion-pairing owing to an absence of explicit solvation or the dynamic notion. For further discussion and examples, see: (a) Sperger, T.; Fisher, H. C.; Schoenebeck, F. Computationally deciphering palladium-catalyzed reaction mechanisms. *Wiley Interdiscip. Rev.: Comput. Mol. Sci.* **2016**, *6*, 226−242, DOI: 10.1002/wcms.1244. (b) Proutière, F.; Schoenebeck, F. Orthogonal Selectivities under Pd(0) Catalysis with Solvent Polarity: An Interplay of Computational and Experimental Studies. *Synlett* **2012**, *23*, 645−648. (c) Lyngvi, E.; Bode, J. W.; Schoenebeck, F. A computational study of the origin of stereoinduction in NHC-catalyzed annulation reactions of α,β-unsaturated acyl azoliums. *Chem. Sci.* **2012**, *3*, 2346−2350.

(38) (a) Bannwarth, C.; Ehlert, S.; Grimme, S. GFN2-xTB−An accurate and broadly parametrized self-consistent tight-binding quantum chemical method with multipole electrostatics and density-dependent dispersion contributions. *J. Chem. Theory Comput.* **2019**, *15*, 1652−1671. (b) Grimme, S.; Bannwarth, C.; Shushkov, P. A robust and accurate tight-binding quantum chemical method for structures, vibrational frequencies, and noncovalent interactions of large molecular systems parametrized for all spd-block elements (Z = 1−86). *J. Chem. Theory Comput.* **2017**, *13*, 1989−2009.

(39) Zou, Y.; Houk, K. N. Mechanisms and Dynamics of Synthetic and Biosynthetic Formation of Delitschiapyrones: Solvent Control of Ambimodal Periselectivity. *J. Am. Chem. Soc.* **2021**, *143*, 11734−11740.

(40) For previous observations of fluoride loss from Pd(II)-F complexes, such as **1**, see: (a) Grushin, V. V. Palladium Fluoride Complexes: One More Step toward Metal-Mediated C−F Bond Formation. *Chem. − Eur. J.* **2002**, *8*, 1006−1014, DOI: 10.1002/1521-3765(20020301)8:53.0.CO;2-M. (b) Grushin, V. V. Generation of "Naked" Fluoride Ions in Unprecedentedly High Concentrations from a Fluoropalladium Complex. *Angew. Chem., Int. Ed.* **1998**, *37*, 994−996.

(41) For spectroscopic observation of $[CF_3\text{-}SiR_3\text{-}F]^-$ at low temperature in solution, see: Maggiarosa, N.; Tyrra, W.; Naumann, D.; Kirij, N. V.; Yagupolskii, Y. L. $[Me_3Si(CF_3)F]^-$ and $[Me_3Si(CF_3)_2]^-$: Reactive Intermediates in Fluoride-Initiated Trifluoromethylation with Me_3SiCF_3 - An NMR Study. *Angew. Chem., Int. Ed.* **1999**, *38*, 2252−2253.

(42) It is worth noting that the CF_3^- anion has been detected in solution and even crystallized with a suitable cation, see: (a) Harlow, R. L.; Benet-Buchholz, J.; Miloserdov, F. M.; Konovalov, A. I.; Marshall, W. J.; Escudero-Adán, E. C.; Martin, E.; Lishchynskyi, A.; Grushin, V. V. On the Structure of $[K(crypt\text{-}222)]^+ CF_3^-$. *Helv. Chim. Acta* **2018**, *101*, No. e1800015, DOI: 10.1002/hlca.201800015. (b) Lishchynskyi, A.; Miloserdov, F. M.; Martin, E.; Benet-Buchholz, J.; Escudero-Adán, E. C.; Konovalov, A. I.; Grushin, V. V. The Trifluoromethyl Anion. *Angew. Chem., Int. Ed.* **2015**, *54*, 15289−15293. (c) Prakash, G. K. S.; Wang, F.; Zhang, Z.; Haiges, R.; Rahm, M.; Christe, K. O.; Mathew, T.; Olah, G. A. Long-Lived Trifluoromethanide Anion: A Key Intermediate in Nucleophilic Trifluoromethylations. *Angew. Chem., Int. Ed.* **2014**, *53*, 11575−11578.

(43) The CF_3SiMe_3F anion could in principle eventually also liberate difluorocarbene via further exchanges (anionic chain process), as studied in detail recently: see ref 14. However, our dynamics simulation of the ion pair $[(PPh_3)_2Pd^{(II)}(Ph)(PhCN)]^+$ $[CF_3\text{-}SiMe_3\text{-}F]^-$, i.e. starting from TS_{rb}, suggested that it would readily collapse to $[(PPh_3)_2Pd^{(II)}(Ph)(CF_3)]$ within 2 ps, during which the CF_3 anion rebounds with the cationic Pd. (No fragmentation of the CF_3 anion to difluorocarbene was observed - in 148 of the 500 trajectories the CF_3 anion remained at a roaming stage within the maximium simulation time of 8 ps. Even if fragmentation were to happen, difluorocarbene

would then be expected to insert into another molecule of **1**, which in turn would give rise to *trans*-$Pd^{(II)}CF_3$ complex and not the observed *cis*-species.)

(44) Our xTB single point energy calculations of the same stationary points indicated that xTB energetically follows the same pathway preference as DFT in favoring the ionic pathway in polar solvent via fluoride abstraction and CF_3 anion rebound. By contrast, for the difluorocarbene releasing pathway (as found to be favored in non-polar medium by DFT), xTB energies suggest different selectivities of the mechanistic pathways. xTB-based difluorocarbene post-transition state dynamics are hence not applicable.

(45) To comment on the energy differences of the various possibilities we speculate the following: The pentacoordinate intermediates change their conformation via a Berry-type pseudorotation mechanism. Due to steric effects the trigonal bipyramids (e.g. III) are energetically favored, whereas square pyramids (e.g. II) are higher in energy. Moreover, the axial positions in the trigonal bipyramid experience increased steric repulsion due to three angles of 90° to their nearest neighbors and only one ligand being located further away at 180°. The equatorial positions are sterically less encumbered (only two 90° angles and two 120° angles). As a result, the large phosphine ligands appear to preferentially orient themselves in the equatorial positions (e.g. in III). Directly comparing the two transition states where solvent (MeCN) dissociates, the two phosphines are axial en route to *trans*-**2** (i.e. more steric repulsion and hence higher in energy), whereas the phosphines are equatorial en route to *cis*-**2** (i.e. experiencing less steric repulsion).

(46) (a) Becke, A. D. Density-Functional Exchange-Energy Approximation with Correct Asymptotic Behavior. *Phys. Rev. A* **1988**, *38*, 3098−3100. (b) Lee, C.; Yang, W.; Parr, R. G. Development of the Colle-Salvetti Correlation-Energy Formula into a Functional of the Electron Density. *Phys. Rev. B* **1988**, *37*, 785−789.

(47) Francl, M. M.; Pietro, W. J.; Hehre, W. J.; Binkley, J. S.; Gordon, M. S.; DeFrees, D. J.; Pople, J. A. Self-consistent molecular orbital methods. XXIII. A polarization-type basis set for second-row elements. *J. Chem. Phys.* **1982**, *77*, 3654−3665.

(48) Andrae, D.; Häußermann, U.; Dolg, M.; Stoll, H.; Preuß, H. Energy-adjusted ab initio pseudopotentials for the second and third row transition elements. *Theor. Chim. Acta* **1990**, *77*, 123−141, DOI: 10.1007/BF01114537.

(49) Grimme, S.; Antony, J.; Ehrlich, S.; Krieg, H. A consistent and accurate ab initio parametrization of density functional dispersion correction (DFT-D) for the 94 elements H-Pu. *J. Chem. Phys.* **2010**, *132*, 154104.

(50) Zhao, Y.; Truhlar, D. G. A new local density functional for main-group thermochemistry, transition metal bonding, thermochemical kinetics, and noncovalent interactions. *J. Chem. Phys.* **2006**, *125*, 194101.

(51) Weigend, F.; Ahlrichs, R. Balanced basis sets of split valence, triple zeta valence and quadruple zeta valence quality for H to Rn: Design and assessment of accuracy. *Phys. Chem. Chem. Phys.* **2005**, *7*, 3297−3305.

(52) Marenich, A. V.; Cramer, C. J.; Truhlar, D. G. Universal Solvation Model Based on Solute Electron Density and on a Continuum Model of the Solvent Defined by the Bulk Dielectric Constant and Atomic Surface Tensions. *J. Phys. Chem. B* **2009**, *113*, 6378−6396.

https://doi.org/10.1021/jacsau.3c00724
JACS Au 2024, 4, 263−275